Journal of Structural Geology 33 (2011) 244–254

Contents lists available at ScienceDirect

Journal of Structural Geology

journal homepage: www.elsevier.com/locate/jsg

Natural annealing of dynamically recrystallised quartzite fabrics: Example from the Cévennes, SE French Massif Central

Clemens Augenstein*, Jean-Pierre Burg

Department Earth Sciences ETH and University Zurich, Sonneggstrasse 5, 8092 Zurich, Switzerland

ARTICLE INFO

Article history:
Received 6 March 2010
Received in revised form
13 October 2010
Accepted 18 October 2010
Available online 5 November 2010

Keywords:
Cévennes
Massif Central
Quartz
CPO
EBSD
Annealing
Dynamic recrystallisation

ABSTRACT

Quartzite samples from the SW-Cévennes (French Massif Central) have been investigated in order to reveal the effects of annealing on a previously dynamically recrystallised quartz fabric. The studied quartzite is interlayered with turbiditic micaschist series, and after regional deformation the whole sequence was intruded by the St-Guiral granodiorite at 1–3 kbar and up to 650–700 °C. Recorded crystallographic preferred orientation (CPO) patterns of the dynamically recrystallised quartzite are classified as type I with a monoclinic symmetry and type II with an orthorhombic symmetry. Type I is related to simple shear-dominated deformation and type II to apparent constriction. These two fabric types are consistent with structural observation that a constrictive and coaxial deformation regime controlled the formation of non-cylindrical and refolded folds. In the metamorphic aureole, which produced essentially static annealing, CPO patterns intensify slightly and grain size increases towards the granodiorite until the temperature at which inversion from low- to high quartz is triggered. This inversion caused a volume increase and subsequent intergranular stresses activated slip systems fitting the temperature and water content.

This study shows that annealing of dynamically recrystallised quartz crystals can activate previously inactive slip systems, reactivate slip systems and amplify older CPO fabrics. This conclusion identifies limits for the use of annealed quartz fabrics in reconstructing structural histories when earlier dynamic recrystallisation has occured.

1. Introduction

The effects of annealing on quartz CPO fabrics have been investigated in several experimental studies (e.g. Green, 1967; Green et al., 1970; Heilbronner and Tullis, 2002) and some natural examples (Park et al., 2001; Piazolo et al., 2005; Otani and Wallis, 2006; Trepmann et al., 2010). The major drawback of experimental studies is the difficulty in extrapolating the process to geological timescales. This is especially the case for the annealing of dynamically recrystallised fabrics. We consider natural dimensions in time and space are essential for understanding and applying quartz fabrics to geological problems, and this can only be achieved by studies on naturally recrystallised and annealed rocks. However, natural examples of recrystallised and subsequently annealed quartz fabrics are rare. Previous studies show very few or no comparisons of annealed versus un-annealed samples in the same geological setting. Park et al. (2001) and Piazolo et al. (2005) describe only one annealed natural sample and do not compare its CPO with those from un-annealed samples. Otani and Wallis (2006) show examples where initial dynamic recrystallisation of quartz took place during a range of high-T/low-P conditions, but only compare the CPOs of a small number of annealed to un-annealed samples. Trepmann et al. (2010) investigated two annealed samples without a direct comparison to un-annealed rocks from the same initial dynamic recrystallisation. In addition to the limited number of samples, previous studies on natural examples just apply the results from experiments thus assuming that annealing has no major effect on previously established quartz CPO patterns.

Our study documents a natural example, where dynamic recrystallisation occured in a in a well-constrained setting and observed quartz fabrics represent dynamically recrystallised and annealed samples. Additionally, we have studied nearly twice the amount of samples analysed in previous studies.

The dynamic recrystallisation recorded in our samples took place during medium-T and medium-P metamorphism and was overprinted by a high-T event related to a granodioritic intrusion.

* Corresponding author. Present at: Research School of Earth Sciences, ANU, Canberra, ACT, 0200 Australia.
E-mail address: clemens.augenstein@anu.edu.au (C. Augenstein).

0191-8141/$ – see front matter © 2010 Elsevier Ltd. All rights reserved.
doi:10.1016/j.jsg.2010.10.008

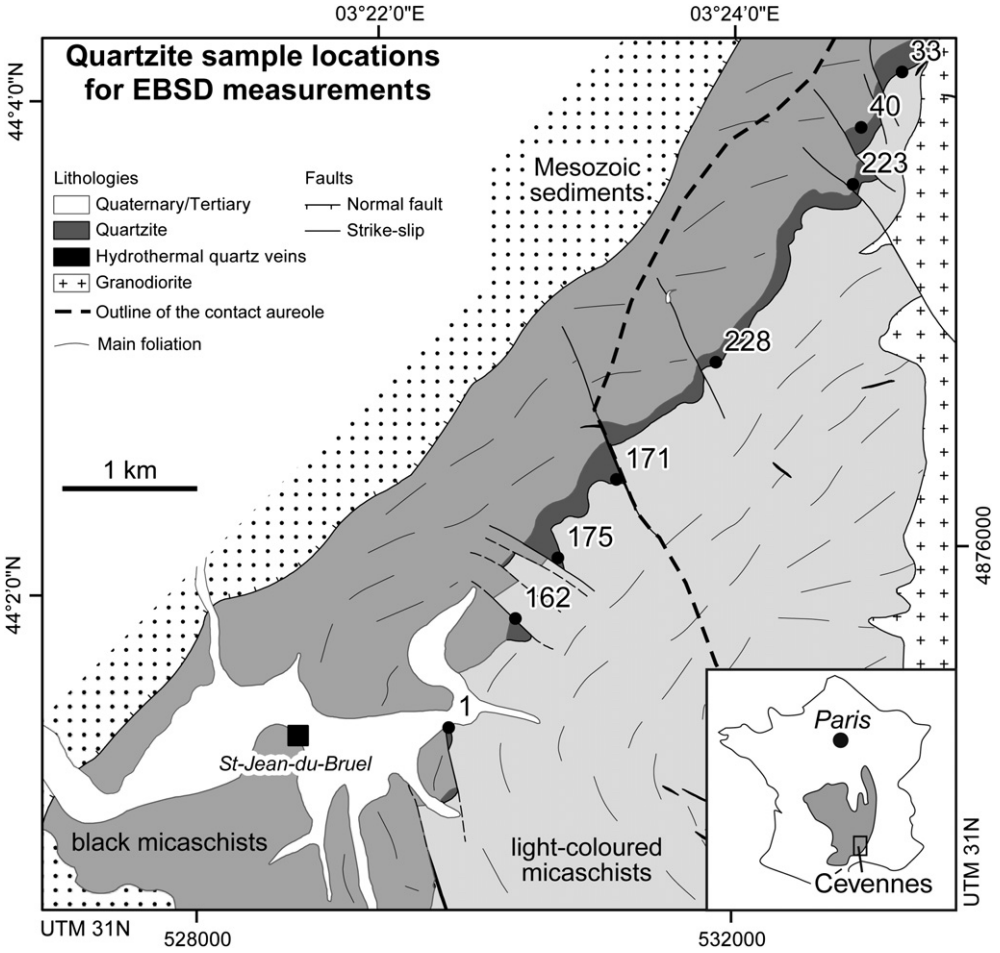

Fig. 1. Geological map of the study area with location of CPOs in Figs. 5 and 6. Inset: location of the Cévennes in the Massif Central and France.

If static annealing changes pre-existing quartz CPOs, the stability of CPOs is questionable, and with it the robustness of the information derived from quartz CPOs in terms of regional kinematics.

The studied quartzite layer extends from the contact to the granodiorite to beyond the contact aureole (Fig. 1). This allows comparison of CPO patterns of dynamically recrystallised samples from outside to inside the contact aureole and so documents the effects of a progressive increase in temperature on static annealing of dynamically recrystallised quartz fabrics. This rare geological setting was chosen to gain new insights into the behaviour of dynamically recrystallised quartz crystals during natural annealing.

Detailed structural and petrological investigations have been carried out in order to set the kinematic context of the CPO patterns that were obtained by electron back scatter diffraction (EBSD) measurements in a scanning electron microscope (SEM) at the Electron Microscopy Center at the ETH Zurich (EMEZ).

2. Geological setting

The study area is located in the SE of the French Massif Central close to the village of St-Jean-du-Bruel and is part of the "Cévennes méridionales" (Fr.: southern Cévennes, Fig. 1). The Cévennes are part of the western European Variscan Belt that resulted from the Devono-Carboniferous collision between Gondwana in the S with Laurussia in the N, and some intervening continental blocks (e.g. Matte, 2001). The Cévennes consist mainly of micaschists, gneisses and several granitic plutons. The micaschists are regarded as the southern para-autochthon on which high-grade thrust sheets were emplaced southward with a displacement of about 200 km during the Variscan orogeny (Burg and Matte, 1978; Matte and Burg, 1981; Ledru et al., 1989; Matte, 1991; Arnaud et al., 2004). The Cévennes micaschists, in turn, have been thrust southward over the so-called

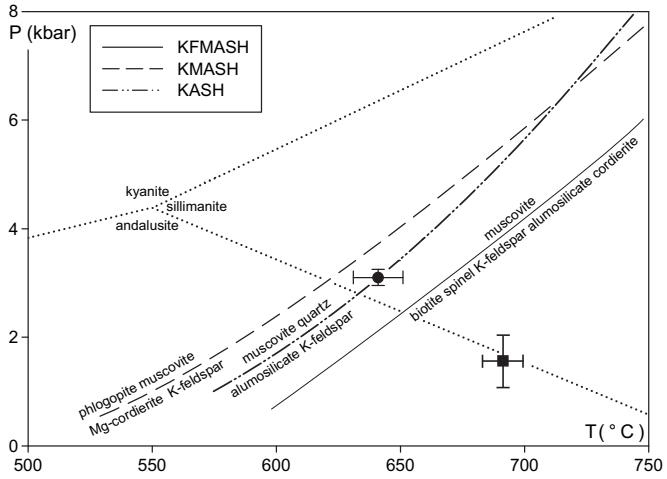

Fig. 2. P-T grid with relevant, calculated KFMASH system reactions plus H_2O at the high-T side. Dot with error bars gives contact metamorphic conditions next to the St-Guiral granodiorite intrusion (GPS: 03°25′2.7″E; 44°2′49,8″N) from this study. Square with error bars: conditions obtained by Najoui et al. (2000) about 3 km north of our sample location. Regional conditions determined by Arnaud (1999) lay out of this diagram, at $T < 500$ °C for P ca. 4 kbar.

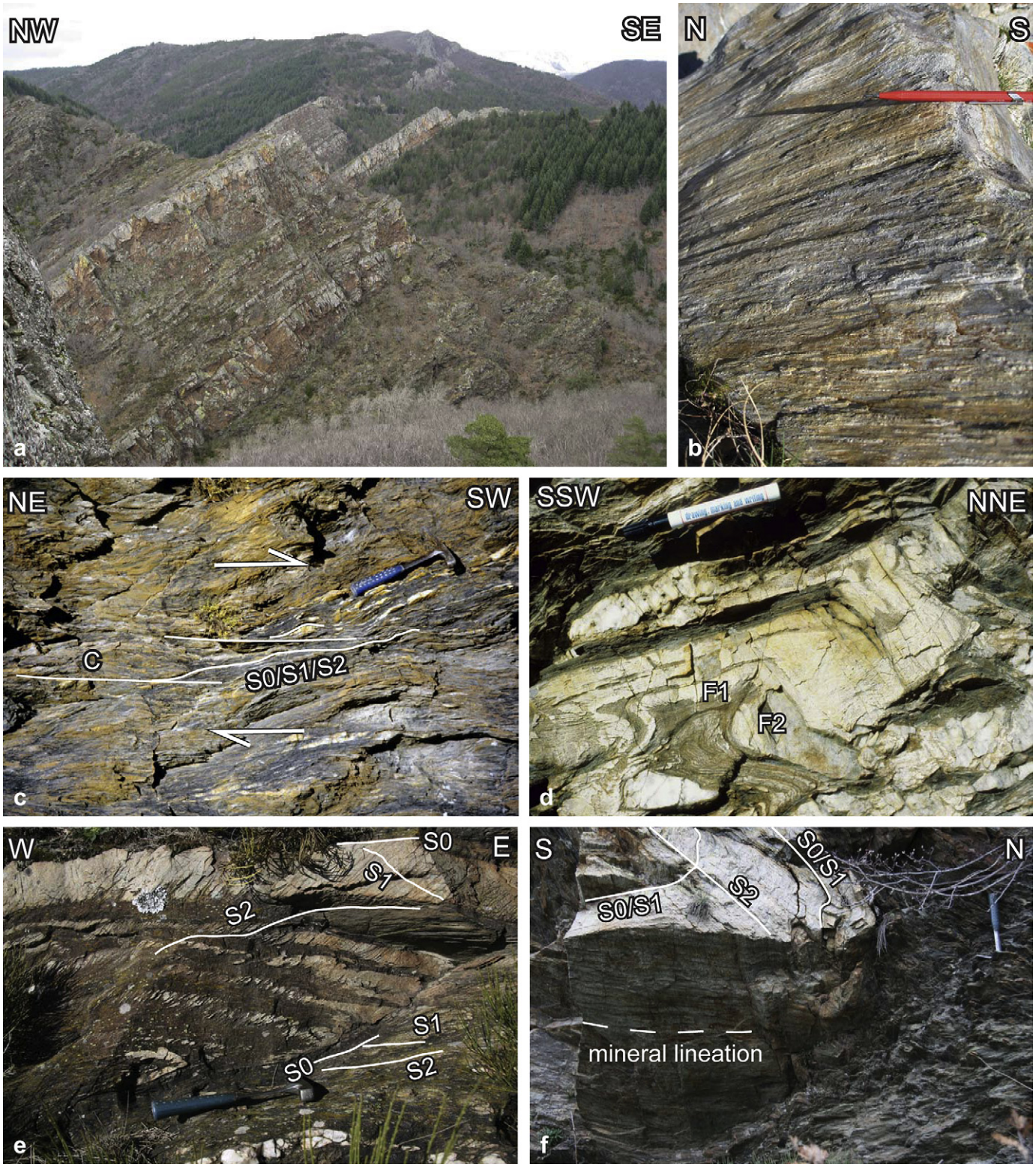

Fig. 3. Images from the study area. a) the studied quartzite layer in normal position between the light-coloured (below) and black (above) micaschist series; b) quartz rods defining the N-S trending mineral stretching lineation in a quartz-rich sequence; c) shear bands (C) in micaschists deflecting the main foliation (S0/S1/S2) and providing evidence for top-to-SW shear; d) cut through a non-cylindrical F2 fold, "refolding" an F1 isoclinal fold; e) F2 recumbent fold with strongly fanning S2 sub-parallel to S0 and S1 in the lower, inverted limb, and markedly oblique to these earlier planar structural elements in the top, normal limb; note thinner bedding on inverted limb indicates stronger shearing f) F2 folds with transverse mineral (elongation) lineation on S2 in the lower, normal limb.

Le Vigan and Monts-de-Lacaunes series (Demay, 1948; Burg and Matte, 1978; Arnaud et al., 2004). The greenschist to lower amphibolite facies metamorphism of the micaschists in the Cévennes méridionales was estimated at 400–500 °C and 4.3 ± 0.4 kbar (Arnaud, 1999) and dated at around 340 Ma (Ar–Ar on biotite and muscovite; Caron, 1990; Faure, 1995) to the NE of the study area. Regional metamorphism was overprinted in most of the Cévennes méridionales by a high-T/low-P metamorphism (>680 °C, 4–5 kbar) at about 325 Ma (Ar–Ar on amphibole and biotite; Najoui et al., 2000). This high-T event was followed by the granodiorite intrusions of the St-Guiral-Aigoual-Liron pluton at 311-306 Ma (U–Pb on zircon and Ar–Ar on muscovite and biotite; Brichau et al., 2008). These granitic intrusions are related to extension at the end of the Variscan orogenesis (Burg et al., 1994; Faure, 1995). The syn- to post-orogenic extension lasted from 320 to 280 Ma (Arnaud et al., 2004). The working area (Fig. 1) includes the western margin of the St-Guiral pluton, which intruded at about 1–3 kbar and 650–700 °C (Najoui et al., 2000; and this study; Fig. 2). The two main metasedimentary formations of the Cévennes micaschists, a black (Cambrian?) and a lighter coloured (Ordovician?) metapelitic and sandy sequence, cover the area. The studied quartzite layer separates the two micaschists, is discontinuous and up to several tens of meters thick (>90% quartz, Fig. 3a) with primary thickness variations. It is of inferred (by lithostratigraphic correlation) Tremadocian

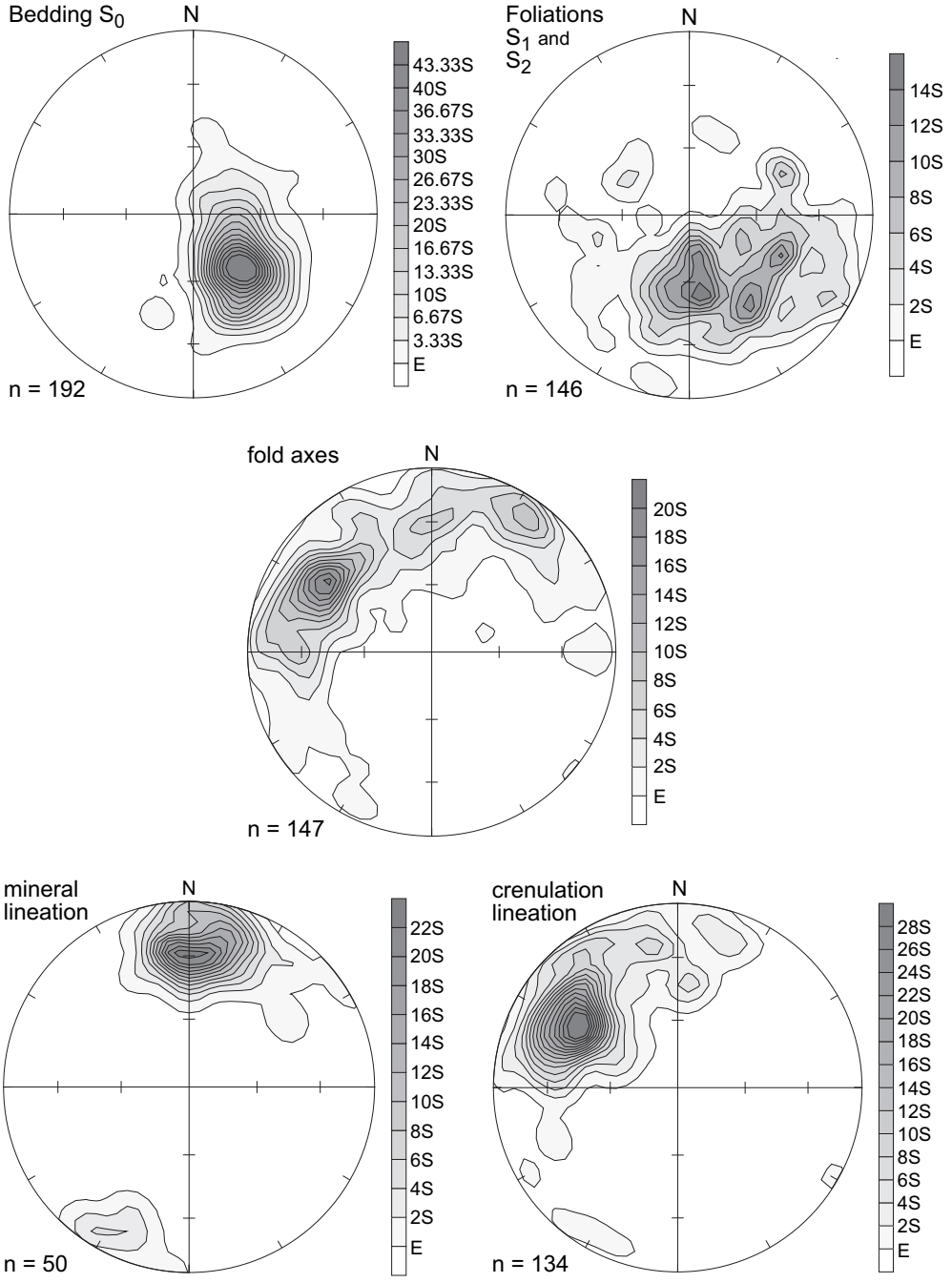

Fig. 4. Lower hemisphere, equal area (Schmidt net) stereoplots of poles to planes S0, S1 and S2 and projection of linear structural elements. Density contours are multiples of the standard deviation S from the mean E. n = number of measurements.

age (Gèze, 1949), although no fossil has ever been found in these rocks.

3. Deformation structures

Bedding (S0) is quite frequently well preserved and regularly dips about 30° towards N–NW (Fig. 4). To the S, the dip direction rotates towards W and SW (Fig. 1).

3.1. Foliation

Two foliations, S1 and S2, are pervasive yet not everywhere easy to distinguish from each other, because S1 is often close to S0 and S2 sub-parallel to S1 (Fig. 3e and f). As a consequence, poles to S1 and S2 are difficult to separate in stereoplot projection (Fig. 4). S2 planes and measurements being regionally a few degrees steeper than N–NW-dipping bedding (Fig. 4) indicate a generally normal sequence and a regional south-southeastward vergence of asymmetrical to isoclinal folds. This association and structural arrangement, along with smaller refraction in inverted limbs, are consistent with a bulk south-southeastward shear.

Depending on the mica content, the morphology of the spaced and often disjunctive foliations S1 and S2 ranges from smooth and parallel in rocks with a low mica content to smoothly anastomosing at a higher content (terminology from Passchier and Trouw, 2005). Domain cleavages of both S1 and S2 contain the same micas, which indicates that they formed during the same metamorphic event. Transitions between cleavage domains and microlithons are discrete in the majority of the samples.

In the microscope, the spaced and disjunctive foliation planes are often overprinted by a steeper S3 crenulation cleavage. This cleavage, which strikes W–E to NW–SE, is the axial plane to NW plunging folds that formed late in the folding history.

3.2. Folds

Three weak maxima of fold axes can be differentiated in stereoplot distributions (Fig. 4): towards 1) NW 2) N–NE and 3) NE-NNE. The F1 and F2 fold axes often belong to overturned to recumbent, cm- to m-scale tight or isoclinal folds, which locally show curved hinges or are refolded (Fig. 3d). The wide distribution along the great circle reflects the fact that F1 and F2 are non-cylindrical.

The N and NE-directed folds are overprinted by usually open, locally tight, NW plunging folds. In places, kink-shaped folds with N- to NE-directed axes overprint the dominant open NW folds and older isoclinal folds. These kink-shaped folds are very late features that may have formed during granodiorite intrusion or later.

3.3. Lineations

A pervasive WNW-plunging crenulation lineation (Fig. 4) is sub-parallel to the NW-plunging folds.

The mineral elongation (elongated quartz rods in the field, Fig. 3b, ribbons in thin section, and mica elongation in thin sections) is generally plunging to the N-NNE on undifferentiated S1 and S2 planes (Fig. 4), to the S-SSW in the southern part of the map area. The narrow plot distribution demonstrates that this lineation has a nearly constant orientation over the map area and generally oblique or transverse to F1 and F2 fold axes. This structural relationship reflects also the non-cylindricity of fold axes.

Sigma-clasts and shear bands (C–S-type fabric, Fig. 3c) are commonly observed on exposures sub-parallel to the mineral-stretching lineation (taken as *X* direction of finite strain; Ramsay, 1967) and orthogonal to the foliation (XY plane of finite strain, ibid.). These shear sense indicators are well developed in the micaschists, rare in meta-rhyolites and even less abundant in the studied quartzite. They systematically indicate a bulk top-to-S-SSW shear direction.

4. Pressure-temperature conditions of deformation and annealing

The regional greenschist to lower amphibolite facies metamorphism (400–500 °C, 4.3 ± 0.4 kbar, ~340 Ma; Caron, 1990; Faure, 1995; Arnaud, 1999) is obliterated by a high-T/low-P event (>680 °C, 4–5 kbar, ~325 Ma) in most parts of the Cévennes méridionales (Najoui et al., 2000). However, the high-T event did not affect the study area where the metamorphic parageneses, out of the contact aureole of the St-Guiral granodiorite, are due to the regional greenschist/lower amphibolite facies metamorphism. The main foliation and mineral stretching direction described in previous paragraphs formed during this regional event.

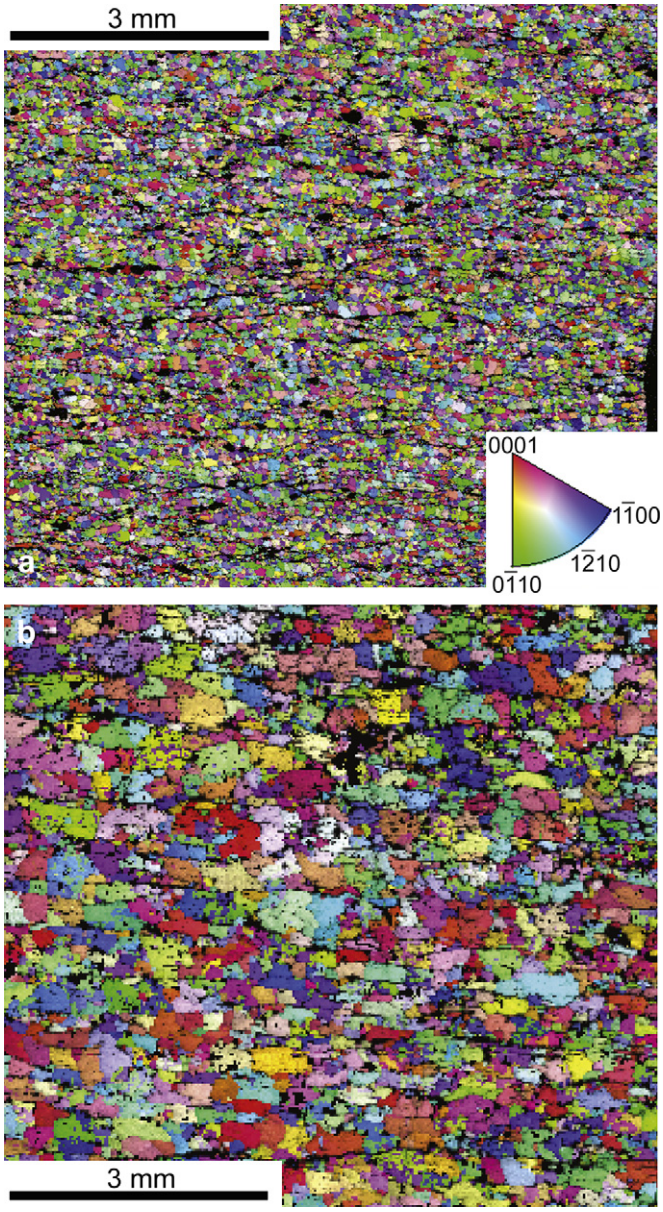

Fig. 5. Crystal orientation maps from a) outside (sample 162) and b) inside (sample 040) the contact aureole. Colour code is for orientation parallel to the N-S trending stretching direction. For both samples N is to the right and S to the left.

In order to specify the annealing conditions, the quantitative analysis of a micaschist sampled few centimetres from the granodiorite was carried out on a "JEOL JXA-8200 Superprobe" at the Institute for Mineralogy and Petrology at the ETH Zurich (analytical information in appendix).

The difference between the P-T conditions of the intrusion of the St-Guiral pluton calculated by Najoui et al. (2000) (690–700 °C on biotite-garnet, 1–2 kbar from garnet-staurolite/cordierite) and our "thermocalc" (Powell and Holland, 1988) based calculation (3.1 ± 0.15 kbar, 641 ± 5 °C; Fig. 2) can be explained by: 1) different sample locations; 2) different methods; and 3) the general problem of precise determination of P (Spear, 1993; Spear and Cheney, 1989; Xu et al., 1994). Most relevant to this study is the temperature determination, which is consistently 650–700 °C at the boundary between the micaschists and the granodiorite.

5. Quartz fabrics

5.1. Method

EBSD patterns were recorded on a SEM with an "EDAX Hikari" camera system (set-up information in appendix). Data acquisition was done by the software "OIM DC5.2", which indexes automatically the collected EBSD patterns and performs the stage and electron beam movements during measurement. Measured fields on the samples were between 1.44 mm^2 and 49 mm^2 with step sizes between 5 μm and 20 μm depending on grain size. Recorded data consists of coordinates (x, y), Euler angles (φ_1, Φ, φ_2) from the EBSD patterns, an image quality parameter (IQ) showing pattern contrast and sharpness of the diffraction band and the confidence index (CI), and an index reliability parameter between 0 and 1. Only quartz was given as a possible phase to the software, so that indexed patterns with a low CI were mainly other minerals (primarily mica) and easy to filter out during data processing. Three cleaning steps were completed as a default operation with the "OIM Analysis 5.2" before calculating pole figures. As a first step the CI of grains larger than 2–5 μm (dependent on the sample's average grain size) was standardized. Afterwards the orientation of neighbouring pixels were correlated with a software intern routine at "clean-up level 1". As a last step, the remaining grains with the same minimum grain size as in the first step were dilated. If necessary, after these three steps, unwanted grains such as remnants of micas or grains of quartz veins formed after dynamic recrystallisation were filtered out using a minimum grain size or CI. Two examples from resulting crystal orientation maps are shown in Fig. 5a (outside the contact aureole) and b (inside the contact aureole).

The cleaned and filtered data was used to plot contoured pole Figs. 6 and 7, and to calculate the grain size distribution in the analysed measurement fields (Fig. 8).

5.2. Microstructures

We found two typical quartz fabrics, which show no correlation to the distance from the intrusion. One of these fabrics is effectively equigranular in thin section (Fig. 9a) with a grain diameter of

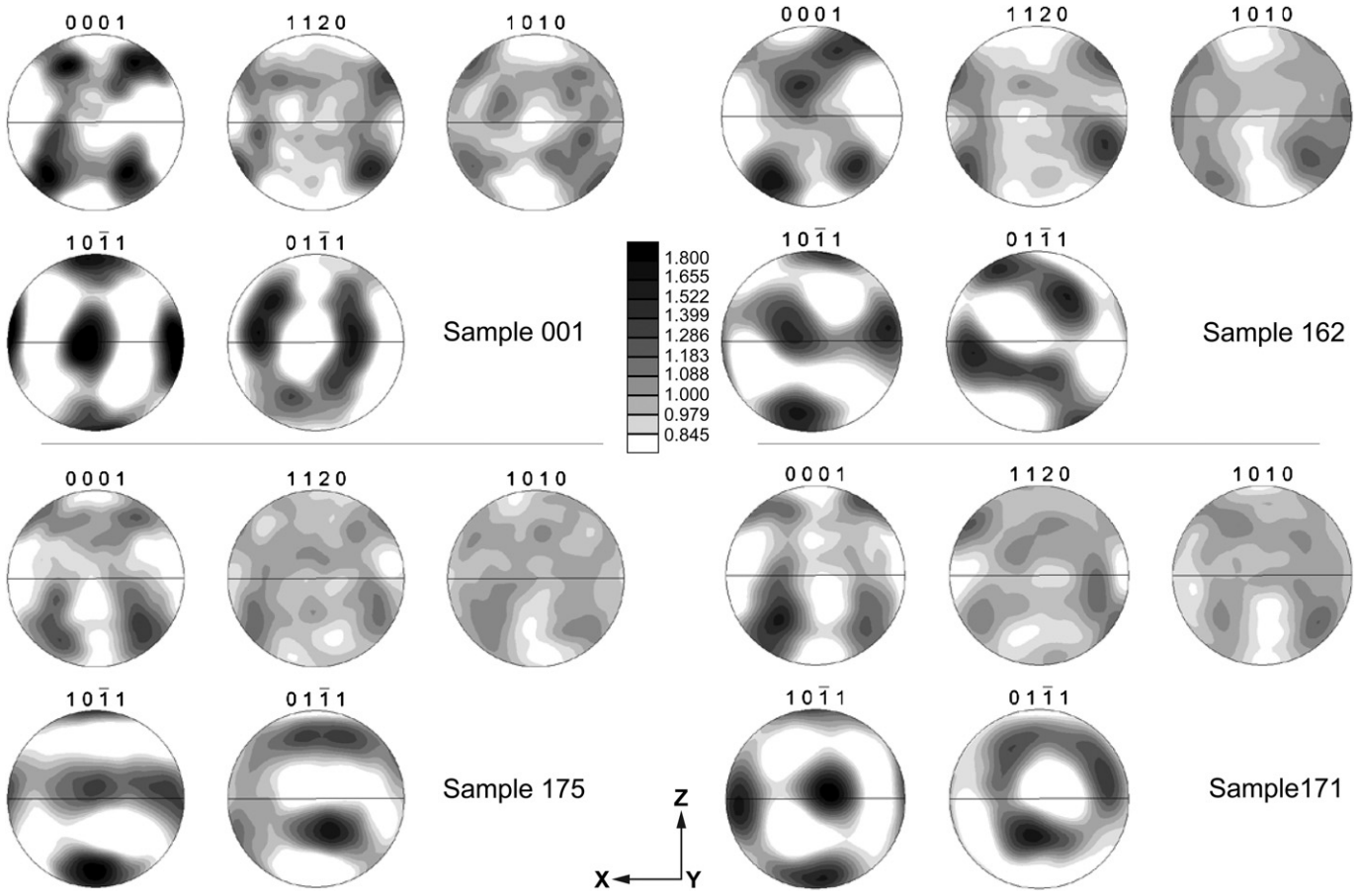

Fig. 6. Stereoplots of quartz crystallographic orientations of samples outside the contact aureole. Horizontal line is the trace of elongation direction X. Z is coplanar and perpendicular to X. The scale is divided in multiples of the uniform distribution. Density distributions were calculated by Gaussian convolution within the harmonic calculus with a smoothing angle of 10°.

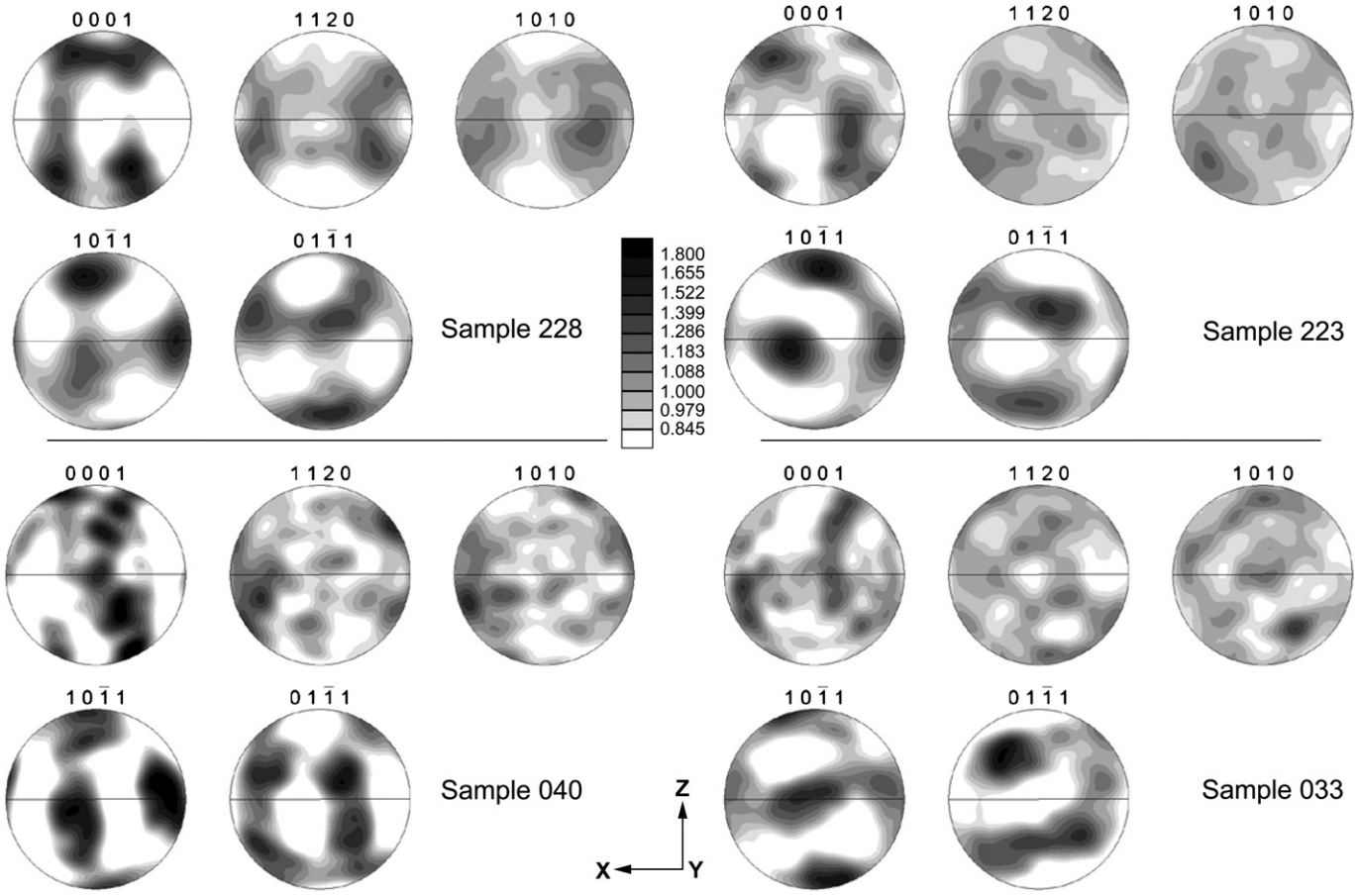

Fig. 7. Stereoplots of quartz crystal orientations of samples inside the contact aureole. Orientation and scaling same as in Fig. 6.

0.02–0.08 mm. The other less frequent quartz fabric shows coarse grains in a fine-grained matrix, where the core is typically 0.2–0.5 mm wide (Fig. 9b). Most of the studied quartzite samples and quartz-rich metapelites possess a well sorted fine-grained fabric with rare coarser grains whose undulatory extinction is more pronounced than that of finer quartz grains. From these observations it can be concluded, that dynamic recrystallisation of quartz in the studied quartzite and quartz-rich metapelites is mainly strain induced grain boundary migration or regime 1 of Hirth and Tullis (1992). The average quartz grain size in the quartzite increases from around 0.05 mm outside the aureole up to 0.25 mm and more at the contact with the granodiorite (Fig. 8). Annealing inside the contact aureole can be inferred to be responsible for the increased grain size and straightening of quartz grain boundaries towards the intrusion.

5.3. Fabrics

Contoured plots show typical patterns of a dynamically recrystallised quartz fabric (Figs. 6 and 7). All stereo plots show weak textures with normally a maximum about twice the uniform distribution. Two types of patterns are recognized:

Type I pole figures (samples 162, 171, 223, 040 and 033) display *monoclinic* textures with c-axis crossed girdles where maxima are mostly concentrated in one girdle. The a-axis fabric also shows one maximum at 90° to the strong girdle of the c-axis cross girdle. The m-plane pole is congruent with the distribution of the a-axes, but with weaker maxima. Maxima of the rhombs are slightly tilted away from the *X*- and *Y*-axis of finite strain.

Type II plots (samples 001, 175 and 228) display *orthorhombic* textures with four maxima for the c-axis and two for a-axes, where the c-axis shows larger angles to the trace of X than a-axes. A- and c-axes patterns have often vertical, slightly curved links between their maxima. The m-plane poles are nearly congruent with the distribution of the a-axis maxima, but are normally weaker. The patterns for the rhombs have a strong orthorhombic symmetry with the maxima close to the X, Y and Z directions of finite strain. The maxima of the rhombs are the strongest.

6. Discussion

6.1. Structures

The macro- and mesoscopic observations document a regional, S–SSW-directed transport direction. The fact that the mineral elongation lineation has effectively a constant orientation throughout the mapping area indicates that the general kinematic direction did not change significantly during the main regional deformation event(s), as is also inferred in other parts of the Cévennes area (e.g. Arnaud et al., 2004). Sub-parallel S1 and S2 are mainly oblique to S0, but can be sub-parallel to it in places. This reflects progressive shearing that generated several successive foliations which formed under the same kinematic and metamorphic conditions. New foliation planes were generated steeper than previous ones on a regional scale (away from hinge zones), yet inclined congruently with the bulk shear movement (Fig. 10). Elongated and oblate minerals (mainly mica) parallel to the shear plane increased the anisotropy of the material. Drag folds that fold

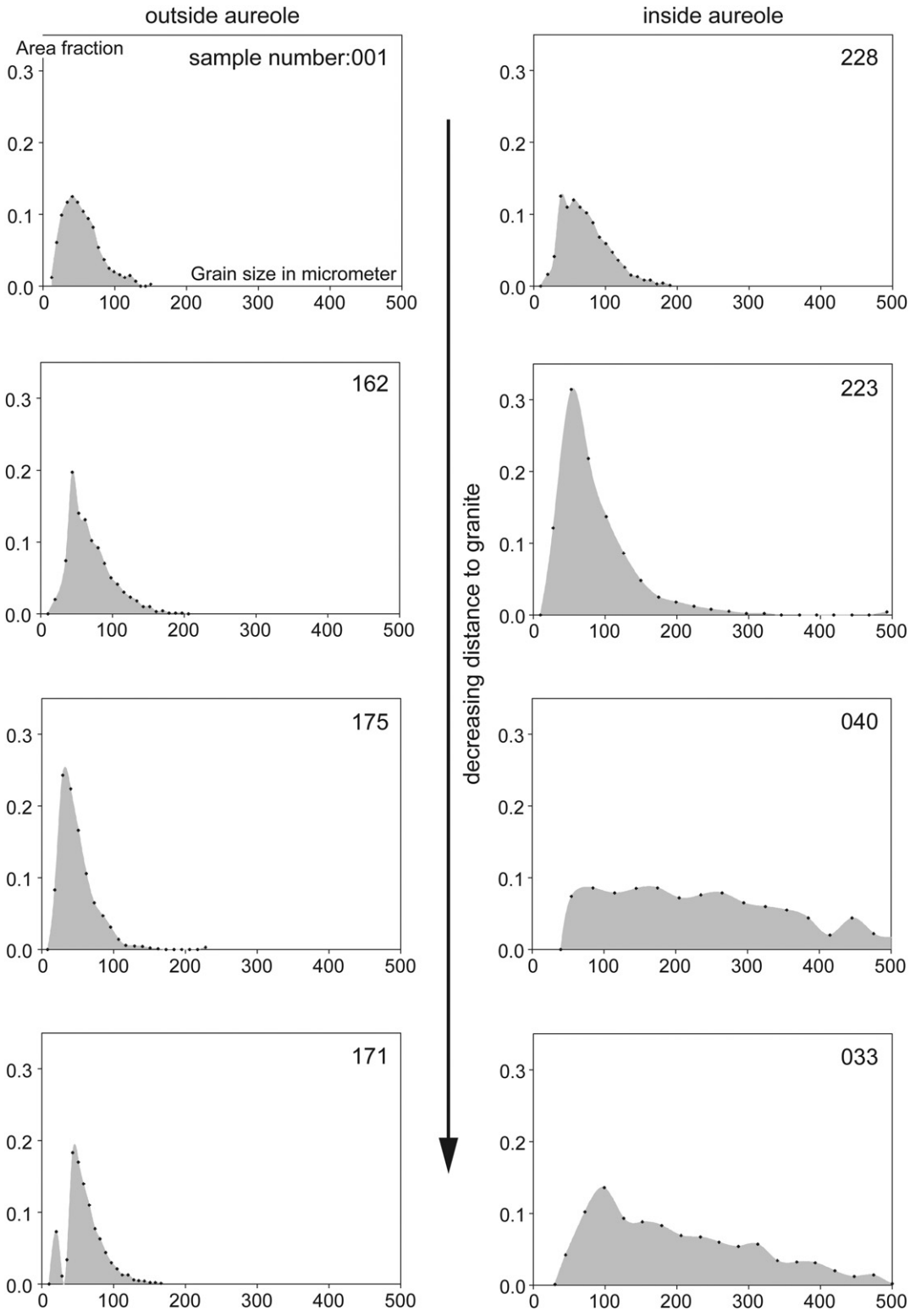

Fig. 8. Grain size distribution in the quartzite samples, calculated from data obtained during EBSD pattern acquisition, showing an increase in grain size towards the granodiorite contact.

bedding and early foliation planes evolved into non-cylindrical folds including the generation of folds and crenulation nearly parallel to the S-SSW movement direction during shearing. Some of the earliest axes of isoclinal "F1" folds, which may have had an initial trend at a high angle to the transport direction, rotated parallel to it with further shearing. Simultaneously, newer "F2" folds were developing at some angle to the stretching-transport direction before being, in turn, rotated towards this direction. This interplay between local folding and regional shearing explains general consistency of curved hinges and refolded folds (Fig. 3d),

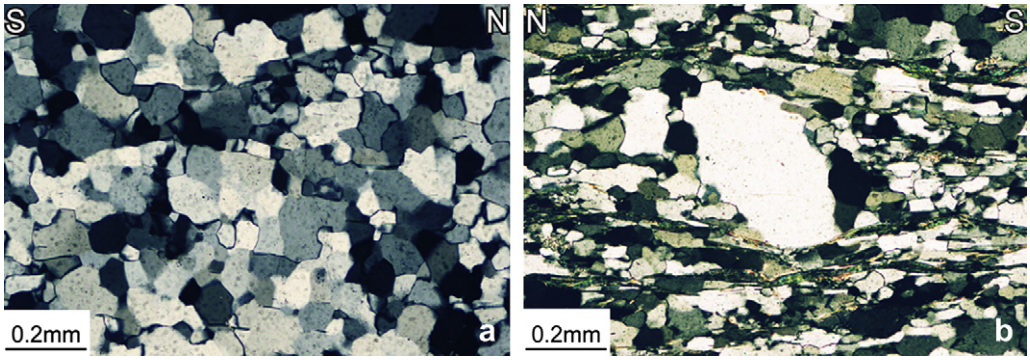

Fig. 9. a) Typical quartz microstructure with equal grain size b) and less frequent with coarse grained core and finer grained mantle.

systematic angular relationships between foliation planes and coherent stretching directions on the regional scale.

The dominant crenulation, NW plunging fold axes and the associated steep cleavage reflect bulk shortening near the *Y* axis of finite strain, hence constriction that folded early foliation around axes generated sub-parallel to the transport direction.

Kinks and flexures are localized overprinting features representing the last stage of deformation. Some of them are related to the granodiorite intrusion.

These structural observations are consistent with the observations of previous authors in the area and the generally accepted orogenic evolution of the Cévennes area (Burg and Matte, 1978; Iniesta, 1980; Meyer, 1990).

The understanding of the structural history (Fig. 10), and with it the conditions during dynamic recrystallisation of quartz, is crucial for comparing the local annealed and un-annealed quartz fabrics and for understanding the effects of static recrystallistation on dynamically recrystallised fabrics.

6.2. CPO

The two types of textures can be related to two deformation regimes. Type I fabrics are associated with simple shear-dominated deformation with low to intermediate strain (Lister and Hobbs, 1980; Schmid and Casey, 1986). The asymmetry of type I fabrics should provide a sense of shear on the most active slip plane (Burg and Laurent, 1978; Lister and Hobbs, 1980). At relatively low metamorphic temperatures of 400–500 °C at a regional scale (Arnaud, 1999; Arnaud et al., 2004) the easiest (and dominant) slip direction in quartz would be <a> (Etchecopar, 1977; Lister and Williams, 1979; Schmid and Casey, 1986; Wenk, 1994). The slip plane contains the a-axis maximum (Lister and Hobbs, 1980; Schmid and Casey, 1986). The position of the c-axis maxima at the periphery of the plots suggests basal <a> slip. C-axis maxima between the center and the periphery indicate rhomb <a> slip. C-axis maxima in the center of a plot point to prism <a> slip (Blumenfeld et al., 1986; Mainprice et al., 1986).

Type II is often inferred to reflect coaxial deformation (Lister and Hobbs, 1980). The strain field responsible for type II patterns plots in a Flinn-diagram in the field between $k = 1$ and $k = \infty$ ($k = [(X/Y)-1]/[(Y/Z)-1]$) (e.g. Lister and Hobbs, 1980; Schmid and Casey, 1986; Passchier and Trouw, 2005). This domain corresponds to a prolate finite strain ellipsoid and represents apparent constriction. The symmetric c- and a-axis maxima result from slip on two conjugate slip planes.

We conclude from the arbitrary distribution of type II and type I patterns over the study area (Fig. 1), that a combination of dominant simple shear and subordinate coaxial deformation led to the obtained patterns. The shear sense from type I plots varies. Samples 162, 171 and also 033 show a top-to-N sense of shear with a strong coaxial component, whereas samples 223 and 040 display a top-to-S movement. These opposite directions can be explained by small-scale (samples are only 2 cm × 3 cm) heterogeneous shearing during drag folding and the subsequent evolution of non-cylindrical folds (see previous paragraphs), which indicate the regional-scale general shear. Furthermore, contradictory shear senses on a microscale are a common observation in low grade shear zones (Hippertt and Tohver, 1999).

The patterns within the contact aureole and close to the granodiorite generally are more clearly defined than those outside the aureole. Examples are samples 001 and 228 for type II, of which 228 shows a little more distinct pattern for apparent constriction than 001. For type I patterns, sample 040 shows more intense effects of shear deformation than sample 162. The stronger patterns could be generated by higher finite strain (Lister and Hobbs, 1980), but the geographical distribution suggests that either contact metamorphism or intrusion related deformation amplified earlier patterns. It is worth noting that the c-axis patterns in the aureole have more maxima in the XY plane, especially in the center of the plot, than samples from outside the aureole. This suggests an increased role of rhomb <a> and prism <a> slip inside the aureole, with basal <a> slip generating maxima at the periphery of the plot (Blumenfeld et al., 1986; Mainprice et al., 1986). This would indicate higher temperature (Blumenfeld et al., 1986; Jessell and Lister, 1990) or higher fluid content (Blacic, 1975) during fabric

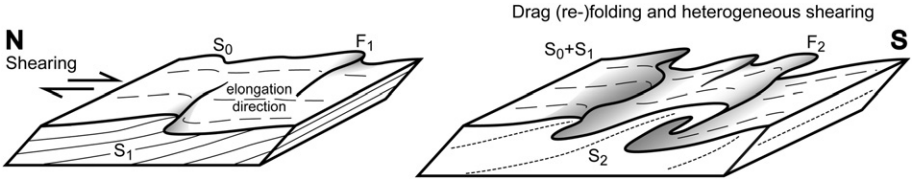

Fig. 10. Sketch of the continuous deformation process under the same N–S shear-dominated regime before granodiorite intrusion in the study area.

generation. The CPO of sample 033 resembles a pattern generated by prism <c> slip in combination with basal, rhomb and prism <a> slip. This is also indicated by the a-axis and m-axis plots, which show maxima not only in the periphery of the plot, but also around (a-axis) and in (m-axis) the *Y* direction. The c-axis slip should relate to high temperature (>650 °C; e.g. Blumenfeld et al., 1986; Jessell and Lister, 1990) and/or high fluid content (Blacic, 1975) during the granodiorite emplacement. The quartzite could have been further deformed along magma borders while increased temperature and/or water content activated other slip systems. However, this effect would be only efficient in the direct vicinity of the intrusion. Another argument against this possibility is that there should be only one deformation expressed in the texture plots, because only the latest stage is preserved (Lister and Price, 1978). At high temperatures <a> and <c> slip is possible at the same time, but the old <a> girdle should rotate en masse towards the new end orientation (Lister, 1981). Yet the pattern of sample 033 (and other samples inside the aureole) does not look like a girdle that rotated as a whole. A better explanation for c-axes parallel to the XY-plane is grain growth and quartz inversion during contact metamorphism. Quartz grain coarsening during contact metamorphism was reported to start at about 620 °C for a pressure of about 3 kbar (Buntebarth and Voll, 1991). These values are close to the metamorphic conditions determined in this study, 650–700 °C and 2–3 kbar. The inversion temperature from low to high quartz at this pressure is about 650 °C (Cohen and Klement, 1967). This inversion is associated with a volume increase, causing intergranular stresses (Wirth, 1985) and enabling activation of prism <c> slip, the high-T environment being likely supported by concomitant dehydration reactions (e.g. Blumenfeld et al., 1986; Jessell and Lister, 1990). Dauphinée-inversion twinning is normally associated to high-low quartz inversion and should be visible in overlapping positive and negative rhomb CPO maxima in the stereoplots (e.g. Tullis, 1970). Only sample 033 displays maxima overlaps in both rhomb plots. This fabric would corroborate our suggestion of quartz inversion in sample 033. Sample 040 exhibits evidence for grain growth (Fig. 8) caused by contact metamorphism, but does not show a CPO pattern comparable to that of sample 033. We assume that sample 040 reached temperatures high enough for quartz coarsening (>620 °C; Buntebarth and Voll, 1991) but still too low to trigger quartz inversion (~650 °C; Cohen and Klement, 1967). It seems that patterns from inside the aureole are slightly more intense than patterns from outside. This observation suggests that annealing of quartz fabrics due to contact metamorphism has a slight amplifying effect. Perhaps, grain growth or raised water content during dehydration reactions in the contact metamorphic aureole caused reactivation of previously active slip systems and hence intensification of the recorded pattern. Alternatively grains with a lower dislocation density, i.e. dynamically recrystallised grains, were favoured during annealing and grain growth at the expense of grains with a higher dislocation density. At this point, the cause for amplification of dynamic recrystallisation patterns in a contact aureole remains speculative and further study is needed.

The results of our study have significant implications for using annealed CPO patterns to deduce deformation history. CPO patterns of dynamically crystallised quartz patterns are insensitive to static annealing (e.g. Heilbronner and Tullis, 2002), if grain growth and/or raised water content from dehydration reactions do not activate previously inactive slip systems, but only reactivate previously used slip systems. Therefore, CPO patterns from annealed quartz fabrics can be used to deduce deformational history only if the annealing conditions match or are lower in temperature and water content than the conditions during dynamic recrystallisation.

7. Conclusions

The structural history responsible for the generation of the dynamically recrystallised quartz fabrics and the later annealing and its effects on the earlier fabrics can be summarized as follows:

1. The Saint-Jean-du-Bruel area deformed under a combination of heterogeneous shearing and folding, creating structures characterized by regional top-to-SSW shear.
2. This combination of simple shear and constrictional deformation produced the quartz fabrics in quartzite. Where general shear had a higher component of coaxial deformation the plot shows an orthorhombic (type II) symmetry. A higher shear component resulted in a monoclinic (type I) symmetry.
3. Subsequent intrusion of a granodioritic body caused annealing in its contact aureole. This triggered inversion from low to high quartz next to the intrusion, and the related volume increase caused intergranular stresses. This inversion altered previously established quartz fabrics because new slip systems were activated.
4. A slight quartz fabric intensification can be observed inside the contact aureole, but more studies of naturally annealed quartzites are needed to understand the significance of this intensification.

These new findings show limits for the use of annealed quartz CPO patterns to deduce a pre-annealing deformation history, because quartz inversion and other processes alterating initial patterns might lead to incorrect conclusions.

Acknowledgements

This work was partly supported by the ETH Zurich. We thank Karsten Kunze for his important contribution in acquiring and understanding the EBSD data sets. Careful and pertinent reviews from G.E. Lloyd, an anonymous reviewer and Dazhi Jiang helped to greatly improve the interpretation and the presentation of our results. Iona Stenhouse and Lloyd White are thanked for polishing the English of the manuscript.

Appendix : EBSD pattern acquisition

EBSD patterns were recorded on a "FEI Quanta 200 FEG" scanning electron microscope with an "EDAX Hikari" camera system at the Electron Microscope Center of the ETH in Zurich (EMEZ). Quartzite chips were cut parallel to the stretching lineation (*X* axis of the finite strain ellipsoid) and perpendicular to the main foliation (XY-plane). The 3 cm × 2 cm sized XZ sample planes were polished with diamond paste down to 1 μm and lapped using a colloidal silica suspension in an automated ultrafine polishing system. The samples were not coated, but edges have been covered with silver paint in order to reduce charging during measurement. Measurements were carried out in low vacuum mode (around 30 Pa) to avoid charging. The pattern acquisition was done with 20 kV acceleration voltage, calculated 7 nA beam current and with a working distance of 15–16 mm on the 70° tilted sample.

P-T data acquisition

The "JEOL JXA-8200 Superprobe" at the Institute for Mineralogy and Petrology at the ETH Zurich operated with a high voltage of 15 kV, an average beam current of 20 nA and beam diameter of 1 μm. Background and peak detection times were 20 s and 40 s, matrix correction was carried out with microprobe internal "CITZAF v3.5" software. The data was normalized with the programs

"CONVERT" and "NORM v6", both written by Peter Ulmer, with the appropriate model for every mineral. Thermobarometric calculations were done with the average P–T method of the free "Pascal" version of "THERMOCALC v3.31" (Powell and Holland, 1988). Calculations were based on minerals of the KFMASH system (Powell and Holland, 1990; Spear and Cheney, 1989).

References

Arnaud, F., 1999. Analyse structurale et thermo-barométrique d'un systéme de chevauchements varisque: Les Cévennes centrales (Massif central français). Documents du BRGM 286 351.

Arnaud, F., Boullier, A.M., Burg, J.P., 2004. Shear structures and microstructures in micaschists: the Variscan Cévennes duplex (French Massif Central). Journal of Structural Geology 26, 855–868.

Blacic, J., 1975. Plastic-deformation mechanisms in quartz: the effect of water. Tectonophysics 27, 271–294.

Blumenfeld, P., Mainprice, D., Bouchez, J.L., 1986. C-slip in quartz from subsolidus deformed granite. Tectonophysics 127, 97–115.

Brichau, S., Respaut, J.P., Monié, P., 2008. New age constraints on emplacement of the Cévenol granitoids, South French Massif Central. International Journal of Earth Sciences 97 (4), 725–738.

Buntebarth, G., Voll, G., 1991. Quartz grain coarsening by collective crystallization in contact quartzites. In: Voll, G., Töpel, J., Pattison, D., Seifert, F. (Eds.), Equilibrium and Kinetics in Contact Metamorphism. Springer Verlag, pp. 251–265.

Burg, J.P., Laurent, P., 1978. Strain Analysis of a shear zone in a granodiorite. Tectonophysics 47 (1–2), 15–42.

Burg, J.P., Matte, P., 1978. A cross section through the French Massif Central and the scope of its Variscan geodynamic evolution. Zeitschrift der deutschen Geologischen Gesellschaft 129, 429–460.

Burg, J.P., Van Den Driessche, J., Brun, J.P., 1994. Syn- to post-thickening extension in the Variscan Belt of Western Europe: modes and structural consequences. Geologie de la France 3, 33–51.

Caron, C., 1990. Premiers résultats de l'étude géochronologique détaillée U-Pb et ^{39}Ar-^{40}Ar des Cévennes (Massif Central). Ph. D. thesis, Academie de Montpellier.

Cohen, L.H., Klement, W., 1967. High-low quartz inversion - determination to 35 kilobars. Journal of Geophysical Research 72 (16), 4245–4251.

Demay, A., 1948. Tectonique antéstéphanienne du Massif central. Mémoires de la service carte géologique de la France, 256 pp.

Etchecopar, A., 1977. A plane kinematic model of progressive deformation in a polycrystalline aggregate. Tectonophysics 39, 121–139.

Faure, M., 1995. Late orogenic carboniferous extensions in the Variscan French Massif Central. Tectonics 14, 132–153.

Gèze, B., 1949. Etude géologique de la Montagne Noir et des Cévennes méridionales. Mémoires de la Société géologique de France (nouv. sér) 24 215.

Green, H., 1967. Quartz: extreme preferred orientation produced by annealing. Science 157, 1444–1447.

Green, H., Griggs, D., Christie, J., 1970. Syntectonic and annealing recrystallization of fine-grained quartz aggregates. In: Paulitsch, P. (Ed.), Experimental and Natural Rock Deformation, pp. 272–335.

Heilbronner, R., Tullis, J., 2002. The effect of static annealing on microstructures an crystallographic preferred orientations of quartzites experimentally deformed in axial compression and shear. In: De Meer, S., Drury, M., De Bresser, J., Pennock, G. (Eds.), Deformation Mechanisms, Rheology and Tectonics: Current Status and Future Perspectives. Geological Society Special Publication, 200, pp. 191–218.

Hippertt, J., Tohver, E., 1999. On the development of zones of reverse shearing in mylonitic rocks. Journal of Structural Geology 21 (11), 1603–1614.

Hirth, G., Tullis, J., 1992. Dislocation creep regimes in quartz aggregates. Journal of Structural Geology 14, 145–159.

Iniesta, G., 1980. Etude microtectonique des terrains hercyniens de la Vallée de la Dourbie (Cévennes Meridionales). Analyse de la deformation finie. Ph. D. thesis, Academie de Montpellier.

Jessell, M., Lister, G., 1990. A simulation of the temperature dependence of quartz fabrics. Geological Society Special Publication 54, 353–362.

Ledru, P., Lardeaux, J.M., Santallier, D., Autran, A., Quenardel, J.M., Floc'H, J.P., Lerouge, G., Maillet, N., Marchand, J., Ploquin, A., 1989. Où sont les nappes dans le Massif central français? Bulletin de la Société Geologique de France 8, 605–618.

Lister, G., 1981. The effect of the basal-prism mechanism switch on fabric development during plastic deformation of quartzite. Journal of Structural Geology 3, 67–75.

Lister, G., Hobbs, B., 1980. The simulation of fabric development during plastic deformation and its application to quartzite: influence of deformation history. Journal of Structural Geology 2, 355–370.

Lister, G., Price, G., 1978. Fabric development in a quartz-feldspar mylonite. Tectonophysics 49, 37–78.

Lister, G., Williams, P., 1979. Fabric development in shear zones: theoretical and observed phenomena. Journal of Structural Geology 1, 283–297.

Mainprice, D., Bouchez, J.L., Blumenfeld, P., Tubia, J.M., 1986. Dominant c slip in naturally deformed quartz: implications for dramatic plastic softening at high temperature. Geology 14, 819–822.

Matte, P., 1991. Accretionary history and crustal evolution of the Variscan belt in Western Europe. Tectonophysics 196, 309–337.

Matte, P., 2001. The Variscan collage and orogeny (480-290 Ma) and the tectonic definition of the Armorica microplate: a review. Terra Nova 13, 122–128.

Matte, P., Burg, J.P., 1981. Sutures, thrusts and nappes in the Variscan arc of western Europe: plate tectonic implications. In: Coward, M.P., McClay, K. (Eds.), Thrust and Nappe Tectonics. Geol. Soc. London, 9, pp. 353–358.

Meyer, V., 1990. Etude Petro-Strutural de la vallée de la Dourbie et de la région de Sauclières (Cévennes meridionales). Ph. D. thesis, Academie de Montpellier.

Najoui, K., Leyreloup, A.F., Monié, P., 2000. Conditions et âges ^{39}Ar/^{40}Ar de mise en place des granitoïdes de la zone externe sud du Massif central français: exemple des granodiorites de St-Guiral et du Liron (Cévennes, France). Bulletin de la Société Geologique de France 171, 495–510.

Otani, M., Wallis, S., 2006. Quartz lattice preferred orientation patterns and static recrystallisation: natural examples from the Ryoke belt Japan. Geology 34, 561–564.

Park, Y., Ree, J.H., Kim, S., 2001. Lattice preferred orientation in deformed-then-annealed material: observations from experimental and natural polycrystalline aggregates. International Journal of Earth Sciences 90 (1), 127–135.

Passchier, C.W., Trouw, R.A.J., 2005. Microtectonics. Springer Verlag.

Piazolo, S., Prior, D.J., Holness, M.D., 2005. The use of combined cathodoluminescence and EBSD analysis: a case study investigating grain boundary migration mechanisms in quartz. Journal of Microscopy-Oxford 217, 152–161.

Powell, R., Holland, T., 1988. An internally consistent dataset with uncertainties and correlations: 3. Applications to geobarometry, worked examples and a computer program. Journal of Metamorphic Geology 6, 173–204.

Powell, R., Holland, T., 1990. Calculated mineral equilibria in the pelite system, KFMASH (K_2O-FeO-MgO-Al_2O_3-SiO_2-H_2O. American Mineralogist 75, 367–380.

Ramsay, J.G., 1967. Folding and Fracturing of Rocks. McGraw-Hill, New York.

Schmid, S.M., Casey, M., 1986. Complete fabric analysis of some commoly observed quartz c-axis patterns. Geophysical Monograph 36, 263–286.

Spear, F., 1993. Metamorphic Phase Equilibria and Pressure-Temperature-Time Paths. In: Mineralogical Society of America, Washington.

Spear, F., Cheney, T., 1989. A petrogenetic grid for pelitic schists in the system SiO_2-Al_2O_3-FeO-MgO-K_2O-H_2O. Contributions to Mineralogy and Petrology 101, 149–164.

Trepmann, C., Lenze, A., Stockhert, B., 2010. Static recrystallization of vein quartz pebbles in a high-pressure-low-temperature metamorphic conglomerate. Journal of Structural Geology 32 (2), 202–215.

Tullis, J., 1970. Quartz - preferred orientation in rocks produced by dauphine twinning. Science 168 (3937), 1342–1344.

Wenk, H.R., 1994. Preferred orientation patterns in deformed quartzites. Reviews in Mineralogy 29, 177–208.

Wirth, R., 1985. The influence of the low high quartz transformation on recrystallization and grain-growth during contact-metamorphism (traversella intrusion, north Italy). Tectonophysics 120 (1–2), 107–117.

Xu, G., Will, T., Powell, R., 1994. A calculated petrogenic grid for the system K_2O-FeO-MgO-Al_2O_3-SiO_2-H_2O. Journal of Metamorphic Geology 12, 99–119.